P7R.11 DOPPLER VELOCITY SIGNATURES OF LARGE-SCALE HYBRID WINDS

Xia Wenmei[1)*], Hu Zhiqun[2)], Tang Dazhang[2)], Liang Mingzhu[3)] and Liu Yuanjian[4)]
1)Jiangsu Institute of Meteorological Sciences, Nanjing 210008, China
2)Nanjing University of Information Science and Technology, Nanjing 210044, China
3)Huzhou City Meteorological Bureau of Zhejiang, Huzhou 313000, China
4)Ji'an City Meteorological Bureau of Jiangxi, Ji'an 343000, China

ABSTRAC

Vast quantities of soundings demonstrate that cold or warm advection is often combined with large-scale convergence or divergence systems. Therefore, analysis is made of features of Doppler radial velocity of the hybrid winds on the velocity PPI charts and effects of raindrop descending speeds on these features by means of numerical simulation. From the simulation charts of variations in divergence and with reference to the related PPI images we obtain convergence or divergence values at all levels from preliminary quantitative analysis.

Keywords: Doppler radar hybrid winds features of radial velocity

1. INTRODUCTION

Concurrently with the launching of Doppler radar deployment and putting into use in China, all kinds of radar products find their wider and wider applications in operational aspects, particularly the product of velocity PPI (plane position indication) for analysis and inference of the structure of an actual wind field.

Normally, the genesis, maintenance and disintegration of a large-scale precipitating system are associated with large-scale convergence and divergence in the mid to lower troposphere, with the convergence (divergence) favorable for rainfall happening or maintenance (ending). Experienced forecasters and weather modification workers can make qualitative judgment of the convergence or divergence condition at all level according to convergence or divergence features on elevated-angle velocity PPI charts, with which to forecast the future weather trend.

The Doppler weather radar is to measure the radial velocity V_r of precipitation particles with respect to the radar, which is related to but different from actual wind speed. The radial speeds are distributed in a complex manner, consisting cold or warm advection, convergence (or divergence) denoted by wind direction/speed, the horizontal velocity V_h and vertical velocity V_f at the level of falling particles, the azimuth α and elevated angle θ of radar beam. From the analysis of radial speeds of single Doppler weather radar for a large-scale rainfall event, we see that most of the data are regarding qualitative convergence or divergence, cold or warm advection, etc. Quantitatively, the dominant product is the VAD-based vertical wind profile (VWP), from which extracted are height-dependent mean wind direction/speed, providing no information on divergence. Following VAD principle, V_f is actually the sum of atmospheric mean vertical velocity W and mean terminal speed of precipitation particles W_0 in a stagnant air in an effective beam striking volume. As a consequence, for radar probing at a high

* *Corresponding author address:* Xia Wenmei, Jiangsu Institute of Meteorological Sciences, Nanjing 210008, China;
e-mail: njxiawm@sina.com.cn

elevated angle, V_f contribution to radial velocity V_r is considerable but V_f uncertainty and its horizontal heterogeneity will lead to greater error in VAD-given horizontal divergence. Only when the radar VAD scan elevated angle is lower or particle vertical speed V_f in the effective beam-striking volume is known, are the vertical structures obtained of horizontal wind direction/speed, divergence and deformation at all levels (Hu et al., 2000).

In the early stage when Doppler radar was put into operation scientists made extensive studies on the features of single Doppler radial velocity. Wood and Brown (1986; 1992), for example, gave many schematic diagrams of such wind fields, which allowed to get an related structure of an real wind field from measured Doppler radial velocity PPI data but the field they used in simulation was relatively simple. On the basis of their study on Doppler velocity images, Xia et al. (2003) conducted a numerical study on Doppler combined velocity images, extracting some features of the wind field of large convergence or divergence combined with cold or warm advection, thereby providing forecasters with assistance in identifying, judging and analyzing the combination. But they did not differentiate between convergence and divergence given as wind speed and direction, nor was account taken of V_f effect. The above efforts allow us to make qualitative judgment of atmospheric convergence or divergence combined with cold or warm advection fields, showing more limitations to operational forecasting.

To get large-scale convergence or divergence values from Doppler radial velocity PPI, numerical study is performed, separately using a wind direction and a speed scheme, on the features of Doppler radial velocity of large-scale convergence or divergence as well as the error in Doppler velocity caused by raindrop falling speed. In practical forecasting, via the identification of the zero-velocity line and other contours, radial velocity V_r in circles at different distance and height and echo intensity displayed on corresponding PPI pictures, which are used to obtain high-precision values of large-scale convergence or divergence by comparing to the simulation charts, avoiding effectively the error from such unsatisfied conditions as V_f uncertainty and horizontal heterogeneity when the elevated angle is high in the use of the VAD technique.

2. MODELING PRINCIPLE AND SIMULATION RESULTS

2.1 Simulation of Convergence or Divergence Displayed by Wind Direction and Speed

The x-axis is set to be positive towards the true north, the y-axis to be positive in the true east, and the z-axis to be positive upward. Next, let the included angle between the horizontal wind and x-axis be θ_0 and we have the expression for $V_r(\theta)$ measured at an azimuth θ and elevated angle α (Hu et al., 2000), viz.,

$$V_r(\theta) = V_h(\theta)\cos\alpha\cos(\theta-\theta_0) - V_f(\theta)\sin\alpha \quad (1)$$

where $V_h(\theta)$ is the horizontal wind velocity and $V_f(\theta)$ is the descending speed of precipitation particles.

Xia et al. (2003) gave Doppler velocity from cold or warm advection combined with convergence or divergence in the form

$$V_r = V_h\cos\alpha\cos\left[\theta-(\theta_0+C_3r)\right]+C_4r \quad (2)$$

in which C_3r is the cold or warm advection

term, denoting that V_h changes with height and because the advection causes the change in wind direction, the strong or weak bending of contours clockwise or counterclockwise on velocity PPI charts shows the features, and $C_4 r$ is the large-scale convergence or divergence term showing effects on V_r at differing distances.

The convergence or divergence term of (2) is the synthesis of convergence or divergence given by wind direction and speed. Besides, no account is taken of V_f impacts on V_r in (2), so that greater errors will arise at a high elevated angle in sounding.

To get rid of the drawbacks we assume V_f to be constant (independent of distance and height); V_h in simulation to be unchanged (its direction is wind direction-denoted convergence or divergence). We set the source to be in the true west and at a distance from the radar y_0. As a result, within the radar reach, wind direction veers clockwise (counterclockwise) on one side of the *y* axis decreases (increases) as a function of the distance and the included angle between the wind and *y*-axis changes as a function of distance. And, on the other side of the *y*-axis, wind veers counterclockwise (clockwise) with distance and the absolute value of the included angle increases (decreases) with distance.

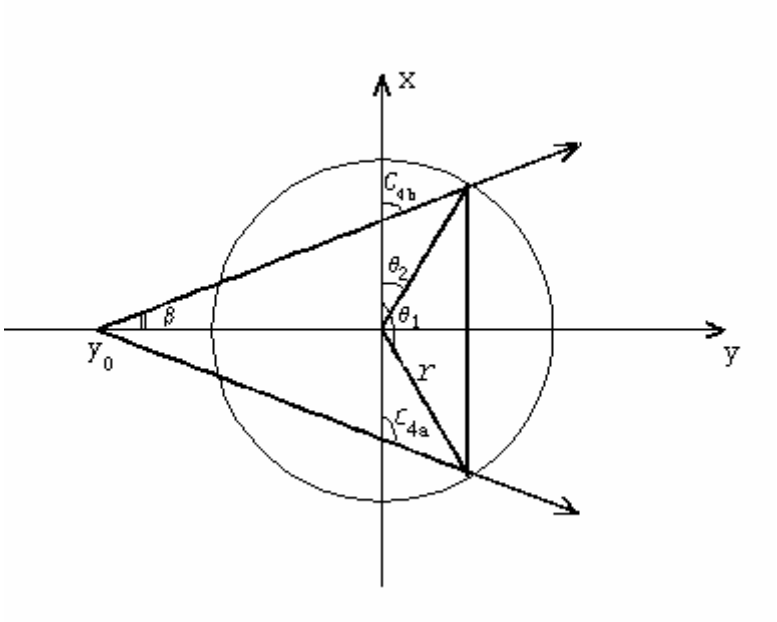

Fig.1. A sketch of large-scale divergence denoted by wind direction.

The Doppler velocity charts for wind direction-given large-scale convergence or divergence display an bow-like zero-velocity line, with convergence (divergence) given by the bow's ends bending towards the positive (negative) speed area for convergence (divergence) (Hu et al. 2000; Xia et al., 2003). The improved expression for Doppler velocity is in the form

$$V_r(\theta) = V_h \cos\alpha \cos\left[\theta - \left(\theta_0 + C_3 r + C_4(r,\theta)\right)\right] - V_f \sin\alpha \quad (3)$$

where $C_3 r$ is the cold or warm advection term and C_4 the large-scale convergence or divergence term, denoting an included angle made between the wind and *x*-axis due to wind direction-given convergence or divergence at a point, and is related to the distance from the radar center *r* and an azimuth θ. C_4 is obtained via

$$\begin{cases} C_{4a} = \dfrac{\pi}{2} + \beta \\ C_{4b} = \dfrac{\pi}{2} - \beta \end{cases} \quad (4)$$

Moreover, using VAD technique we find the divergence of the wind field of the form (Hu et al., 2000).

$$div\mathbf{V_h} = \frac{a_0}{r\cos\alpha} - \frac{2V_f \sin\alpha}{r\cos\alpha} \quad (5)$$

wherein a_0 is the zero-power term of Fourier coefficient.

Take for example warm advection combined with convergence or divergence at elevated angle α=5.0^0. C_3 =0.008 km^{-1} is set and wind veers clockwise from southerly to westerly as a function of height and the convergence or divergence source is set to be away from the radar center at y_0 =300km, V_h =20m/s and V_f =0m/s (not allowing for effects of falling particles). The field for (4) ~ (5) – imitated warm advection combined with wind direction-shown convergence or divergence and Doppler velocity PPI charts are presented in Figs.2 and 3, respectively.

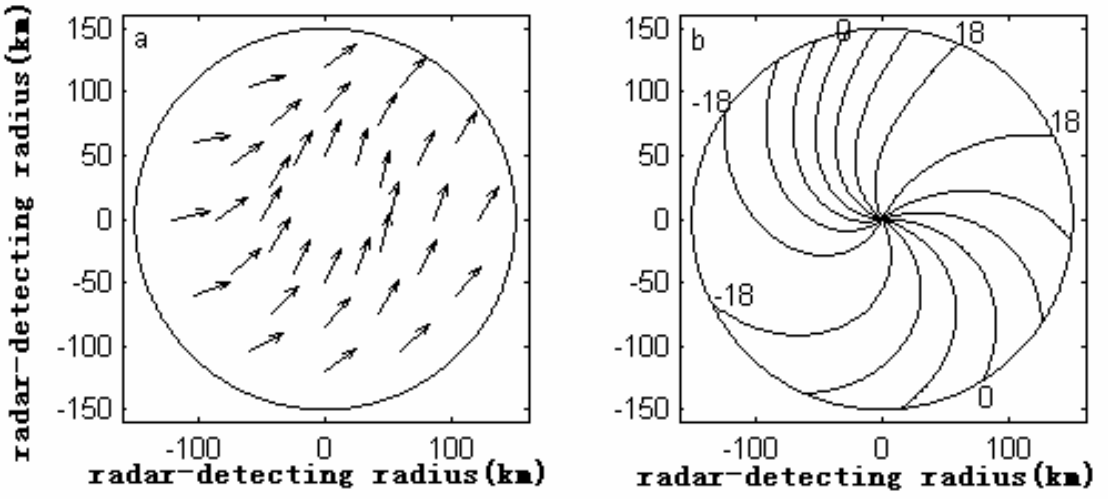

Fig.2 The flow field of wind direction-given convergence with warm advection in a) and Doppler velocity PPI diagram in b).

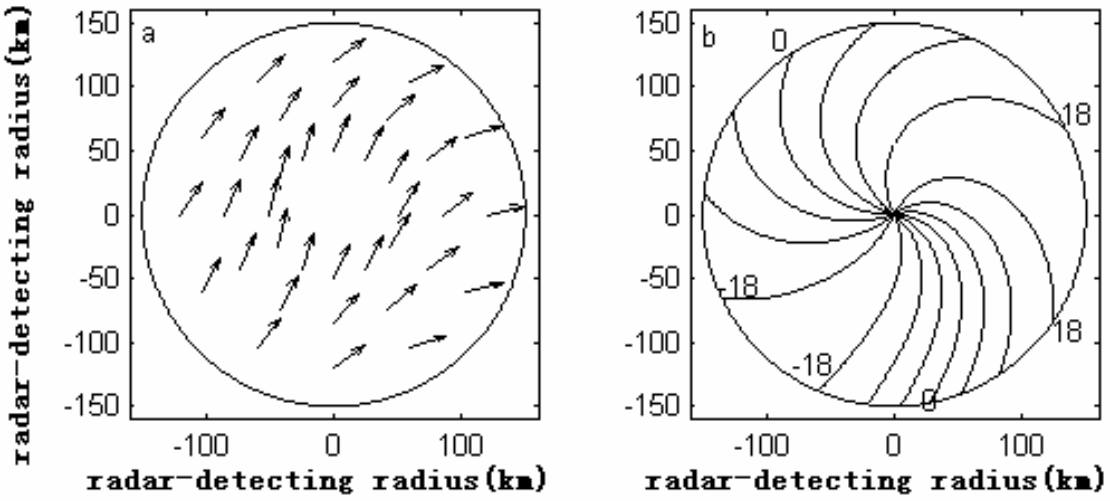

Fig.3. as in Fig.2 except for warm advection combined with wind direction denoted divergence.

Fig.2 shows that the wind (for warm advection plus wind direction-denoted convergence) veers clockwise as a function of distance, with the zero-speed line in an 'S' form on Fig.2b, differing in bending on both sides of the display center. The zero velocity line increases (decreases) its clockwise bending towards the positive (negative) velocity zone with distance on one (the other) side (Xia et al., 2003), leading to the area of negative velocity greatly exceeding that of positive velocity.

Fig.3 depicts the wind (warm advection plus wind direction-given divergence) keeps clockwise veering with distance, and the zero speed line is S-form on the PPI diagram, but its clockwise bending increases (decreases) towards the area of negative (positive) velocity with distance on one (the other) side, leading to the fact that the region of negative velocity is considerably smaller compared to that of positive speed.

In routine work, in identifying a divergence value according to the velocity PPI chart, we are not permitted to have the distance y_0 between convergence or divergence source and radar center. But at a different-point on y_0 the included angle differs between zero-speed lines and other contours.

At distance r, the included angle between zero-speed lines is $\Delta\theta$ and from (3) we find

$$\Delta\theta = \theta_1 - \theta_2 = 2\arccos\left(\frac{V_f}{V_h}\tan\alpha\right) + C_{4a} - C_{4b} = 2\arccos\left(\frac{V_f}{V_h}\tan\alpha\right) + 2\beta \qquad (6)$$

$$\begin{cases} C_{4a} = \dfrac{\pi}{2} + \beta = \dfrac{\pi}{2} + \left(\dfrac{\Delta\theta}{2} - \arccos\left(\dfrac{V_f}{V_h}\tan\alpha\right)\right) \\ C_{4b} = \dfrac{\pi}{2} - \beta = \dfrac{\pi}{2} - \left(\dfrac{\Delta\theta}{2} - \arccos\left(\dfrac{V_f}{V_h}\tan\alpha\right)\right) \end{cases} \qquad (7)$$

which indicates that for a circle the included angle formed from two zero points to the radar center relates to falling particle velocity, Doppler elevated angle, horizontal wind speed and wind direction-shown convergence or divergence at the level of the circle, independent of the intensity of cold or warm advection and horizontal wind

direction. Therefore, by identifying the included angles between zero-speed lines at circles we get the distance between radar center and convergence or divergence source related to the large-scale convergence or divergence, and then against simulations we have divergence values, and the zero-speed line bending towards the positive (negative) area for convergence (divergence).

We set wind speed to be independent of height and azimuth, V_h to be constant and V_f = 0m/s (without falling speed of particles considered). Using the VAD technique and (3)~(5), simulation is made of divergence values in the included angle at different elevated angles, wind speeds and distances. For space limitation given here are only the imitation charts for wind direction-shown convergence at elevation angles of 1.5^0 and 5.0^0, and V_h = 10 m/s in Fig.3, and the associated wind direction-shown divergence has the same values but an opposite sign. The straight lines in Fig.4 stand for the circles at 30, 60, 90 and 120 km away from the radar.

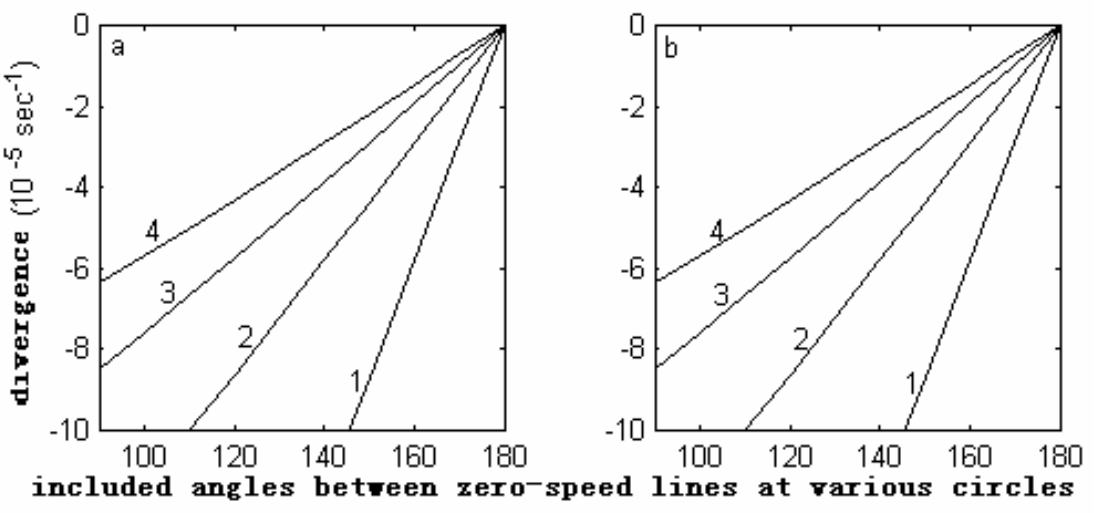

Fig.4. Wind direction-shown convergence values at the different distances (see above) and elevated angles = 1.5^0 and 5.0^0 in a) and b), respectively.

Fig.4 shows that 1) for the same circle, the smaller the included angle between zero speed lines, the larger the convergence value; 2) as the distance is increased the value reduces in the same included angle; 3) the value is independent of change in the elevated angle

According to the VAD principle and with no effect of falling velocity of precipitating particles considered, the divergence bears a linear relation to wind speed, so that with V_h known, the divergence value is to be V_h/10 from Fig.4, other parameters being identical.

2.2 Simulation of Wind-Speed-Given Convergence or Divergence

For the same circle the positive or negative velocity is different in value, leading to wind speed-shown convergence or divergence with negative speed being larger (smaller) than positive speed for convergence (divergence, see Hu et al. 2000).

The simulation field is of west winds, with the direction unchanged versus height. The velocity increases and afterwards decreases

to the east and west of the radar and the maximum wind V_{max} is greater to the east than to the west. Set the wind at surface and model top (h-top) to be zero and h_{vmax} denotes the height at which wind reaches maximum. Below it the wind velocity change is set to be

$$V_h = V_{\max} - \frac{V_{\max}}{h_{v\max}^2}(h - h_{v\max})^2 \qquad (8)$$

and above h_{vmax}

$$V_h = V_{\max} - \frac{V_{\max}}{(h_{top} - h_{v\max})^2}(h - h_{v\max})^2 \qquad (9)$$

Assume V_f = 0 (with no effect of falling particles considered), elevation angle = 5.0^0, and h_{vmax} to be at 5 km level both to the east and to the west except for V_{max} = 20 (40) m/s to the west (east), with wind at surface and 15 km above *msl* being zero. From (8) – (9) we find the height-dependent wind speed to the east and west in Fig.5a. And wind speed-shown convergence (divergence) velocity PPI charts are illustrated in Figs.5b.

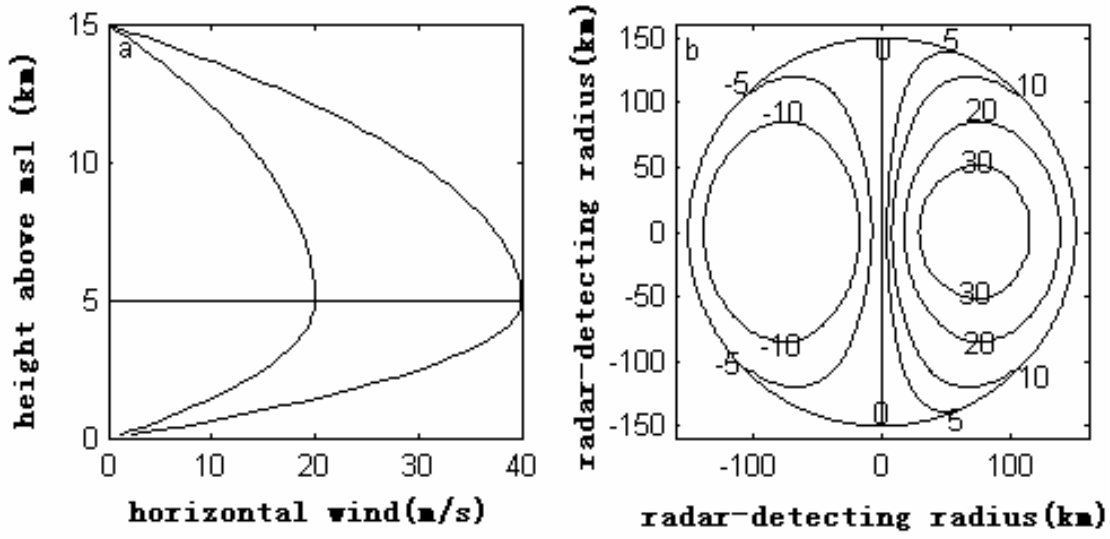

Fig.5. Simulation images of height-varying winds.

Figs.5b shows that with no wind direction-given convergence or divergence present, the included angle between zero speed lines is 180^0 but owing to V_{max} differs to the east and west, different-value positive (negative) radial velocity center would result to the east (west) for wind-speed-shown convergence (divergence).

Set the simulation done to be at elevated angle of 0.5^0 and 5.0^0, negative > positive velocity, and the maximum wind at 3 and 5 km level. We get wind-speed denoted convergence and divergence values for circles at different distances, as shown in Figs.5a,b, respectively. Similarly, with negative < positive speed for divergence, the values are identical but the sign is opposite.

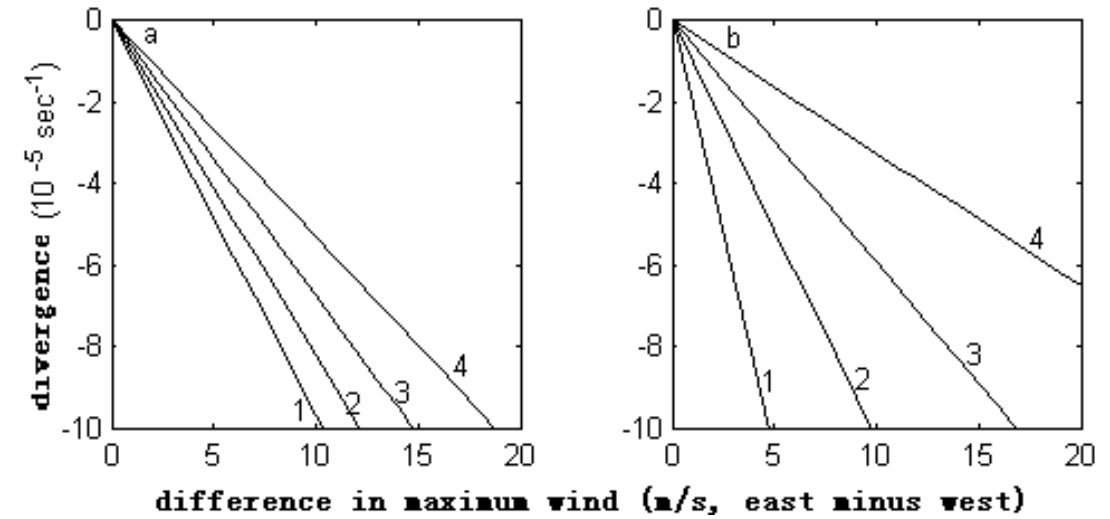

Fig.6. Convergence (divergence) values caused by the difference in 3-km-level V_{max}) (east minus west) for circles at different elevation angles and distances.

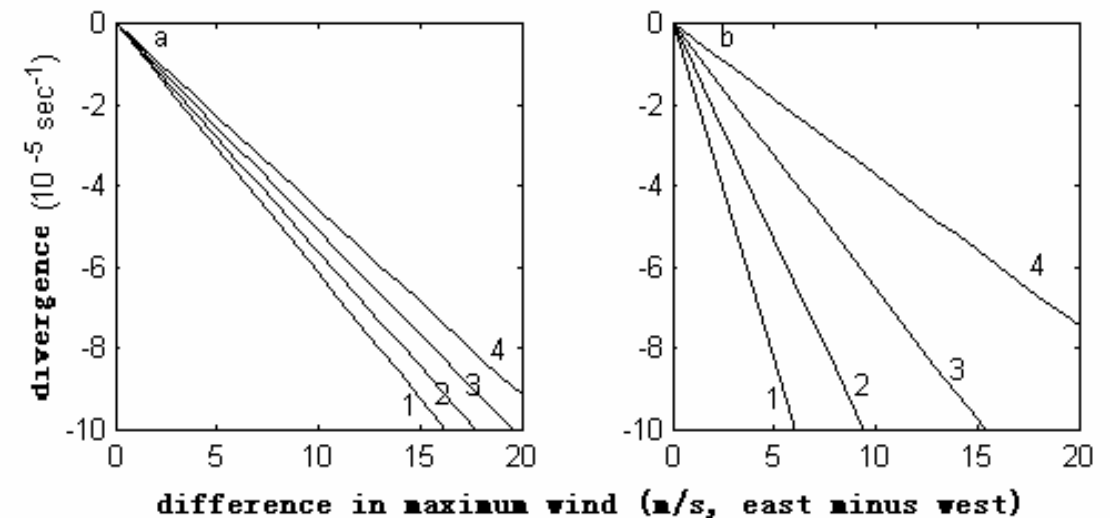

Fig.7. as in Fig.6 but for the 5 km level.

Inspection of the figures yields that 1) for the same circle the increase of difference (east minus west) in V_{max} leads to the increase in divergence values; 2) divergence values decrease for the same difference as a function of distance; 3) with increased elevation angle, wind-speed-denoted divergence values increase at the same distance; and 4) divergence values differ for different h_{vmax}.

2.3 Impacts on Divergence of Falling Velocity of Particles

From (1) and (3), we see that V_f effects are innegligible at high elevated angles. In our simulation, wind direction and speed are independent of azimuth and height. Fig.8 presents the wind velocity PPI charts with V_h = 10 m/s and V_f = 5 m/s at elevated angles of 1.5^0 and 5.0^0. Fig.9 depicts different V_f caused convergence values at different circles.

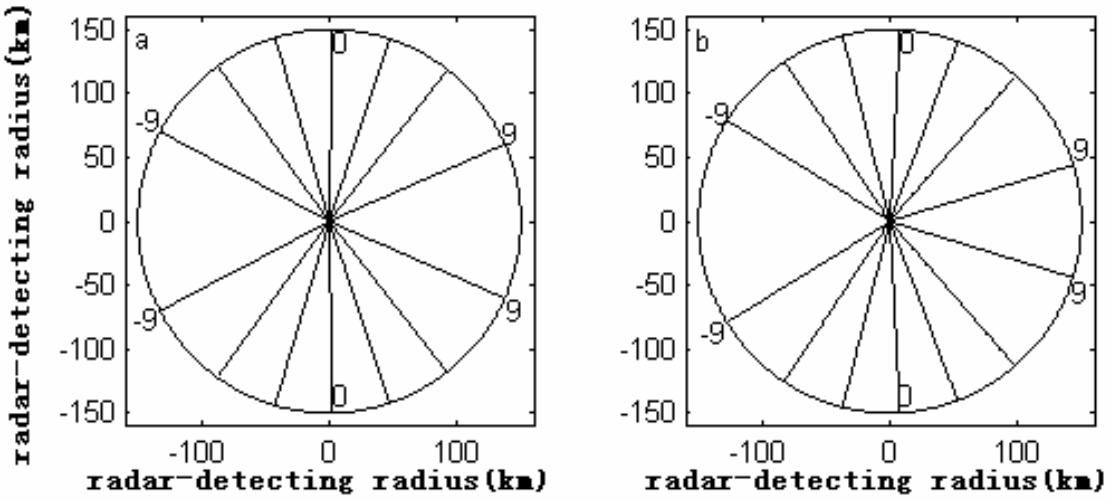

Fig.8 Charts for V_f impact on velocity PPI at V_h = 10 m/s,

with elevated angle of 1.5^0 and 5.0^0 in a) and b), respectively.

Fig. 8 shows that from the velocity PPI chart at elevated angle of 1.5^0 (5.0^0) the included angle between the zero-speed lines is close to 180^0 ($<180^0$), with the contour marked bending towards the positive value area, leading to the area of negative velocity exceeding that of positive velocity. And the curvature will be greater, the bigger the elevation angle. Following the VAD principle, when the elevation angle increases, so does the $V_f \sin\alpha$ of (1) and (3), meaning the increase in the radial component of V_f. For sounding at high elevated angles, the V_f contribution to V_r is significant, leading to bigger errors of VAD-gained horizontal convergence values.

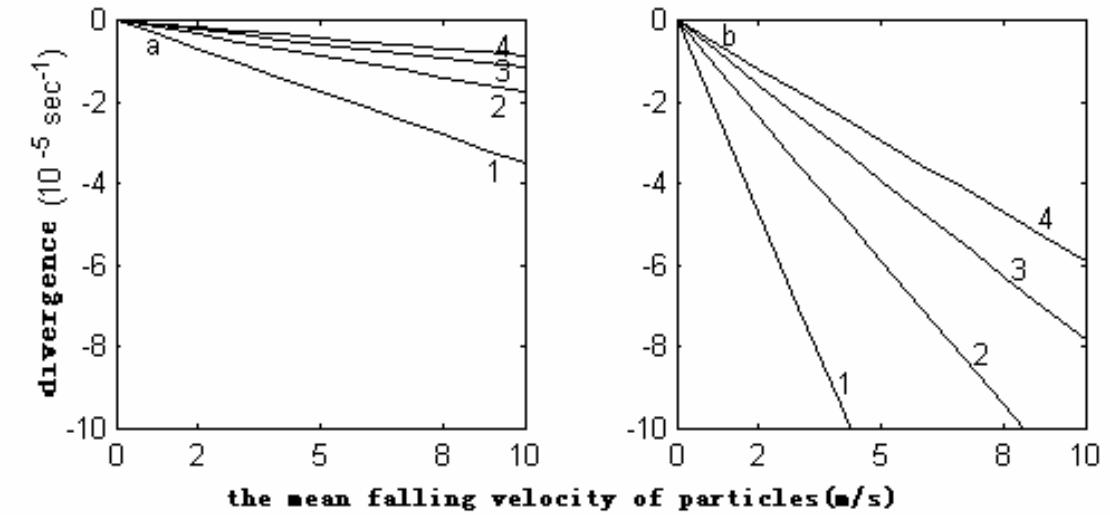

Fig.9. V_f caused convergence values at elevated angle of 1.5^0 and 5.0^0,

respectively, in a) and b).

Fig.9 illustrates that 1) for the same circle V_f increase leads to the increase of convergence values; 2) increase in distance results in the decrease of the convergence value at the same V_f , and 3) when elevated angle is increased, the V_f caused convergence values increase at rapidity for the same distance.

.

3. DISCUSSION

1) The Doppler radial velocity field is quite complicated, consisting of cold or warm advection, wind direction/speed-given convergence or divergence, horizontal velocity at the height of falling particles, their descending velocity, radar azimuth and elevation angle. In making prediction, separate recognition should be made of values of wind direction and speed-denoted convergence or divergence on radar images against simulation charts obtained at different elevated angles, heights and distances, with which to get divergence values. Errors of the divergence values are reduced by means of the empirical expression for particle falling velocity.

2) The included angle between zero speed lines is recognized on circles at different distances and elevated angles on the velocity PPI charts to get wind direction-denoted convergence or divergence values by means of the charts, and further determination is made of the zero speed line-related region for positive (convergence) or negative (divergence) values.

3) The difference (positive minus negative) in V_{max} centers on the velocity PPI chart is found and then the height (h_{vmax}) is obtained from the elevation angle to get values of wind speed-given convergence or divergence by use of the PPI charts.

4) It is necessary to identify mean echo intensity in a circle based on related PPI chart, and the mean falling velocity of particles in the circle is calculated with the empirical expression $V_f = 3.8Z^{0.072}$ and found against the related chart are particles falling-caused false convergence values, which are used to recognize and correct wind direction/speed-denoted convergence or divergence values. Simulation made by Thomas and Srivastava (1991) demonstrates that the falling velocity based on the empirical expression yields the error of 2m/s. Consequently, in making forecasts, error analysis should be made of reduced divergence values by means of divergence values at V_f = 2 m/s in Fig.9. Further introduction is beyond the scope of this work.

5) From Eq.(3) we see that the intensity of cold or warm advection leads only to change in the curvature of contours of positive or negative velocity, not modifying the included angle between zero speed lines and other contours, nor maximum radial velocity, which have no effect on identifying wind speed/direction denoted convergence or divergence.

6) If Doppler velocities available are incomplete and errors from the use of EVAD are greater, then the divergence values can be extracted using the image recognition technique, which is today widely applied in prediction.

ACKNOWLEDGEMENT This work is supported jointly by National Natural Science Foundation of China (40475017) and the Science and Technology Administration of Jiangsu Province (BS2003054).

REFERENCES

Hu Mingbao, Gao Taizhang, and Tang Dazhang, 2000: Analysis and Applications of Doppler Weather Radar Data, China PLA Press, 62-140 pp. (in Chinese).

Hu Zhiqun, Tang Dazhang, Liang Mingzhu et al., 2005: Calculation of atmospheric vertical velocity using improved EVAD and variational scheme, *J. Najing Institute of Meteorology*, **28** (3), 344-350 (in Chinese).

Thomas, M. and R. C. Srivastava, 1991: An improved version of the extended velocity – azimuth display analysis of single Doppler radar data, *J. Atmos. & Oceanic Technology*, **8** (4), 453-456.

Wan Rong and Tang Dazhang, 2002: Comparison of two VAD algorithms and their applications, *J. Nanjing Institute of Meteorology*, **25** (5), 648-655 (in Chinese).

Wood, V. T. and R. A. Brown, 1986: Single Doppler velocity signature: Interpretation of nondivergent environmental winds, *J. Atmos. & Oceanic technology*, **3** (1), 114-128.

Wood, V. T. and R. A. Brown, 1992: Effects of radar proximity on Single Doppler velocity signatures of axisymmetric rotation and divergence, *Mon. Wea. Rev*., **120**, 2798-2807.

Xia Wenmei, Zhang Yaping, Wang Lingzhen et al., 2003: Single Doppler velocity features of hybrid wind fields, *Acta Meteor. Sinica*, **23** (2), 209-216 (in Chinese).